



# Synthesis of mesoporous carbon-polymeric hybrid material for energy storage application

Mijun Chandran<sup>1</sup> · I. Shamna<sup>1</sup> · A. Anusha<sup>1</sup> · Margandan Bhagiyalakshmi<sup>1</sup> 

© Springer Nature Switzerland AG 2019

## Abstract

The overarching goal of this study is fabrication and evaluation of mesoporous carbon-polymeric hybrid electrode materials derived by in situ polymerization of aniline on mesoporous carbon. The mesoporous carbon (CMK-3) was prepared using mesoporous silica SBA-15 as a hard template. The characteristics and functional groups of synthesized mesoporous carbon-polyaniline composite confirmed by Fourier-transform infrared spectroscopy, Raman spectroscopy, Thermo gravimetric analysis, X-ray powder diffraction, and BET surface area analysis. The electrochemical performance of carbon-polyaniline composite was evaluated through its supercapacitor behavior in the electrolyte Potassium bicarbonate ( $\text{KHCO}_3$ ). Synthesized carbon-polyaniline was used as the working electrode after modification with Nafion solution on glassy carbon electrode. The hybrid material reveals high current density with increased storage efficiency due to uniform confinement of polyaniline into the pore structure of CMK-3. The high specific capacitance of 487 F/g was observed on carbon-polyaniline electrode at 0.2 A/g in  $\text{KHCO}_3$ , and also reveals better stability, retained 90% efficiency after 1000 charge–discharge cycles. Thus, the prepared carbon-polyaniline composite exhibit as a good candidate in supercapacitor application.

**Keywords** Mesoporous carbon · Polyaniline · Cyclic voltammetry · Supercapacitor · Energy storage

## 1 Introduction

Recent days, there exist greatest challenges in the developing energy storage system that could efficiently harness energy produced from various renewable energy sources influenced by the location and time. Thus, it is highly desirable to develop energy storage system with high efficiency, high energy storage capacity and low cost so that the stored energy can be used for portable electronic devices and hybrid electric vehicles [1, 2]. Among various energy storage system, batteries and supercapacitors are considered as excellent candidates. As far as batteries are concern can accommodate large energy with poor cycle life [3], whereas, supercapacitors can provide large power density and long cycle life with better charge–discharge properties [4]. The supercapacitors are performed

based on the interaction between the active electrode materials [5] and electrolyte. Hence, the supercapacitor studies provide an opening to explore new possibilities of electrode materials as well as electrolyte. Previous reports demonstrate that the transition metal oxides and conducting polymers are successful electrodes materials for supercapacitors due to their predominantly fast and reversible surface for charge storage [1, 5–9]. Also, conducting polymers like polypyrrole and polyaniline (PANi) have been well-established as electrode material in supercapacitor applications, in terms of flexibility, high conductivity, and synthetic process [10–13]. Especially, polyaniline has attracted great interests in energy storage, sensors, and electrochromic devices because of the simple synthesis route [14] and doping/de-doping chemistry [15], low cost, high conductivity, and excellent

✉ Margandan Bhagiyalakshmi, mbhagija@gmail.com | <sup>1</sup>Department of Chemistry, Central University of Kerala, Kasaragod, Kerala 671316, India.



environmental stability. However, the conducting polymer suffers limited stability during cycling results in declined performance [16]. The limitations of conducting polymer are minimized by making it as composites with carbon materials like mesoporous carbons, CNTs and graphene [17–20], which resulted in the enhanced surface area, high conductivity, and excellent stability. Carbon materials have high capacity for charge accumulation in electrochemical double-layer, and the highest capacitance values can be correlated with surface area, total pore volume [21, 22]. Based on this, CMK-3 derived from mesoporous silica SBA-15 [23] with high surface area, and pore volume which has wide applications in energy storage systems, adsorption, and catalysis [24–27] is chosen as support material for preparation of PANi-carbon composite. However, there are reports available on CMK–PANi composite materials as electrode materials (non-metallic) in supercapacitors. Still, there exists a research gap with respect to synthesis method, choice of electrolyte, etc., which provoked us to carry out studies on CMK-3/PANi composites for Supercapacitor application.

In this study mesoporous carbon material (CMK-3) was synthesized using SBA-15 and surface carboxylation was done by acid digestion, polyaniline was incorporated on carboxylated CMK through in situ polymerization of aniline. The CMK–PANi composite obtained was fabricated on glassy carbon electrode and used as a working electrode to study the supercapacitor behavior in bicarbonate electrolyte. The synergistic effect of PANi and well-ordered mesoporous carbon (CMK-3) endows the composite with high electrochemical capacitance and excellent cycling stability.

## 2 Experimental

### 2.1 Synthesis of CMK-3 from SBA-15

CMK-3 was derived from SBA-15 as per the reported procedure [28, 29]. The molar composition of the reaction mixture was 1 TEOS: 0.017 P123: 5.87 HCl: 0.0025 TMB: 183 H<sub>2</sub>O. Briefly, 4 g Pluronic P123 polymer was dissolved in 150 mL 1.6 M HCl at 40 °C (pH < 2), with rapid stirring. After complete dissolution of the polymer, swelling agent (0.3 g TMB) and inorganic precursor 9.2 mL TEOS added into the mixture and stirred at 40 °C for 8 h. The entire mixture is then transferred to a Teflon bottle, sealed and aged at 80 °C for 24 h. Thereafter, the mixture was cooled then filtered by vacuum filtration and the white powder obtained. The white powder is allowed to dry in air under vacuum for 24 h. The dried as-synthesized sample was calcined in air at 550 °C for 6 h with a heating rate of 1 °C/min. The final product denoted as SBA-15.

The synthesized SBA-15 used as a template for synthesis of CMK-3 [30]. Typically, 2 g of SBA-15 dispersed into aqueous solution of sucrose (0.017 mol), 0.01 mol H<sub>2</sub>SO<sub>4</sub> added to the mixture. Initially, the mixture was heat treated in the oven at 100 °C for 6 h and subsequently heated at 160 °C for another 6 h. The sample turned black, the procedure was repeated with aqueous sucrose (0.01 mol), and H<sub>2</sub>SO<sub>4</sub> (0.005 mol) for complete infiltration and carbonization of sucrose solution into the pores of SBA-15. The carbonization was completed by pyrolysis at 900 °C with a heating rate of 1 °C/min under N<sub>2</sub> atmosphere. The carbon–silica composite obtained after pyrolysis was washed twice with 5 wt% hydrofluoric acid at room temperature, to remove the silica template. The template-free product, CMK-3 was filtered, washed with ethanol, and dried.

### 2.2 Synthesis of CMK–PANi composite

The synthesized CMK-3 (1 g) was carboxylated by treating with nitric acid and recovered product was dispersed in water and ultrasonicated for 30 min. After that aniline ( $4 \times 10^{-2}$  mol) was added into the above solution at 0–5 °C and stirred for 30 min. Then, the pre-cooled ammonium persulphate solution was added drop by drop under stirring to initiate the reaction. The mixture was allowed to react for 3 h with continuous stirring in the ice bath. The black-green product (CMK–PANi) formed was filtered and repeatedly washed with de-ionized water, and ethanol then dried under vacuum.

### 2.3 Characterization techniques

Powder X-ray diffraction patterns were recorded using a Rigaku Miniflex diffractometer with Cu-K $\alpha$  radiation ( $\lambda = 0.154$  nm). The diffraction data were recorded in the  $2\theta$  range of 0.5–10° at 0.02° step size and 1 s step time. The nitrogen adsorption–desorption isotherms were measured at –196 °C on a Micromeritics ASAP 2010 volumetric adsorption analyzer. Before each adsorption measurement, the samples were evacuated at 105 °C under vacuum for 4 h in the degassing port of the adsorption analyzer. The specific surface area ( $S_{\text{BET}}$ ) was determined from the linear part of the BET equation, and the pore size was calculated using the Barrett–Joyner–Halenda (BJH) method. Fourier Transform Infrared (FTIR) spectra of the samples were recorded at room temperature on a Perkin Elmer spectrometer equipped with an ATR (attenuated total reflection) cell. TGA analyses were carried out in N<sub>2</sub> atmosphere at a flow rate of 20 ml/min, on STA 6000 Thermal Analyzer - Perkin Elmer, by heating 5 mg of materials from 25 to 900 °C in steps of 10 °C/min.

## 2.4 Fabrication of working electrode using CMK–PANi composite

The mixture containing 80 wt% CMK–PANi composite, 10 wt% acetylene black, and 10 wt% polytetrafluoroethylene (PTFE) was mixed well in a vial with few drops of acetone and two drops of Nafion solution. The above mixture was ultrasonicated for about 1 h and then coated on the glassy carbon electrode polished with diamond and alumina solution. The fabricated electrode was dried in air dry and used as a working electrode to study the electrochemical properties.

## 2.5 Electrochemical study of fabricated CMK–PANi electrode

Electrochemical measurements have done on SP 240 Bio-Logic electrochemical workstation. The experiments were carried out using a three-electrode cell, in which platinum and Ag/AgCl electrodes were used as counter and reference electrodes, respectively. Cyclic voltammogram of CMK–PANi fabricated electrode in 1 M  $\text{KHCO}_3$  was obtained at different scan rates (i.e. at 1, 2, 5, 10, 20, 50 and 100 mV/s). Galvanostatic charge/discharge behavior was studied at different cycles at a different current density in 1 M  $\text{KHCO}_3$ . Electrochemical impedance spectroscopic measurement also obtained from the fabricated electrode.

## 3 Results and discussion

### 3.1 Characterization

Figure 1 shows the XRD patterns of pristine CMK-3, PANi, and CMK–PANi composite. The inset figure shows the low angles XRD patterns of SBA-15 and CMK-3, exhibited the characteristics peaks at  $2\theta = 0.8^\circ$ ,  $1.5^\circ$ , and  $1.8^\circ$ , and displayed the presence of (1 0 0), (1 1 0), and (2 0 0) planes due to the well-ordered hexagonal mesosphere [31], which indicates that the CMK-3 is a replica of the template SBA-15. CMK-3 and CMK–PANi composites exhibited a broad characteristic diffraction peak at  $2\theta = 23^\circ$  and a low-intensity peak at  $43^\circ$  attributed to the clusters carbon states as fragments of graphene planes and disorganized carbon [32, 33]. The intensity of CMK–PANi composites less when compared CMK-3 which is due to the confinement of PANi inside CMK-3. Figure 1c also shows that pure polyaniline exhibits a low crystallinity of PANi due to the benzenoid and quinoid rings in PANi Chain and correspond peaks at  $14.4^\circ$ ,  $25.42^\circ$ ,  $19.8^\circ$  and  $24.75^\circ$ . The high capacity for charge accumulation in electrochemical double-layer and appreciable capacitance values of CMK–PANi composite reveals the uniform incorporation of PANi inside the

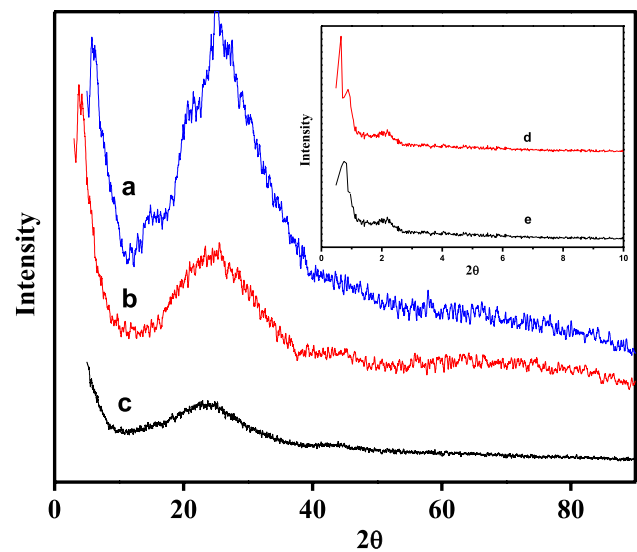


Fig. 1 XRD patterns of (a) CMK–PANi composite, (b) CMK-3, and (c) PANi inset figure (d) SBA-15 and (e) CMK-3

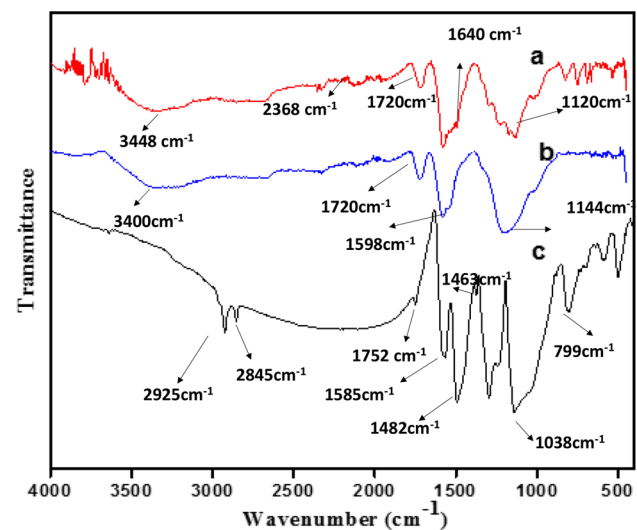


Fig. 2 FT-IR spectra of (a) CMK, (b) CMK–PANi and (c) PANi composite

crystalline CMK-3 without any destruction during in situ polymerization.

Figure 2 shows FT-IR spectra for CMK-3, PANi, and CMK–PANi composite. CMK-3 exhibits characteristics band around  $3400\text{ cm}^{-1}$  attributed to  $-\text{OH}$  stretching and bending vibration of  $-\text{COOH}$  groups at  $1586\text{ cm}^{-1}$ . The bands observed at  $2368\text{ cm}^{-1}$ ,  $1723\text{ cm}^{-1}$ ,  $1578\text{ cm}^{-1}$  and  $1120\text{ cm}^{-1}$  were assigned  $\text{C}=\text{C}$  stretching,  $\text{C}=\text{O}$  stretching vibrations of non-aromatic carboxylic group, aromatic ring stretching vibrations coupled with keto group and  $\text{C}-\text{C}-\text{O}$  bond respectively. The characteristic peaks in PANi: The absorption peaks observed at  $2925\text{ cm}^{-1}$  and  $2845\text{ cm}^{-1}$

are due to asymmetric C–H and symmetric C–H stretching vibrations. The peaks at  $1752\text{ cm}^{-1}$  correspond to C=N stretching mode for imine. The peaks at  $1585\text{ cm}^{-1}$  and  $1482\text{ cm}^{-1}$  are related to C=C stretching vibration for quinoid and benzenoid rings, respectively. The peak at  $1038\text{ cm}^{-1}$  is attributed to C–N stretching mode for benzenoid ring, and the peak at  $788\text{ cm}^{-1}$  is assigned to the plane bending vibration of C–H, which is formed during protonation. In CMK–PANi composites, the carboxyl bands at around  $1723\text{ cm}^{-1}$  depict the hydrogen bonding of PANi with the carboxyl groups on the surface of CMK-3.

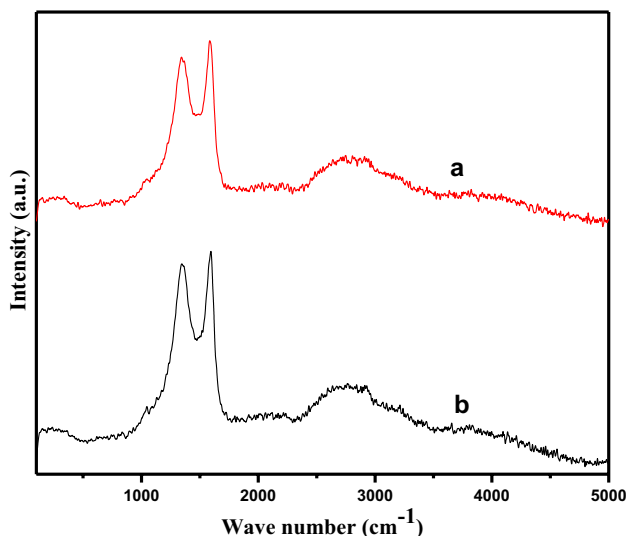


Fig. 3 Raman spectra of (a) CMK-3 and (b) CMK–PANi composite

Also, CMK–PANi composite, the characteristics peaks at  $1574\text{ cm}^{-1}$  correspond to the quinoid ring and the benzene ring while the bands in the range  $1200\text{--}1400\text{ cm}^{-1}$  and  $1144\text{ cm}^{-1}$  correspond to the C–N stretching bands of an aromatic amine [32, 34] and N=Q=N stretching. Thus, the presence of characteristics band in CMK–PANi composites confirms the confinement of PANi in CMK-3. Raman spectra of both CMK-3 and CMK–PANi composite shows broad Raman peaks at  $1590\text{ cm}^{-1}$  (G-band) that indicated the presence of  $E_{2g}$  mode of graphite and is related to  $sp^2$ -bonded carbon atom vibrations (Fig. 3). The other band at  $1350\text{ cm}^{-1}$  (D-band) demonstrated the defects within carbon textures that evidenced the presence of disordered graphite carbon [35] which is in agreement with XRD data. The intensity ratio of both G and D band is nearly 1.

Figure 4A, B shows the  $N_2$  adsorption–desorption isotherms and pore size distribution of CMK-3 and CMK–PANi composite and their textural properties were summarized in Table 1. The functionalized CMK-3 by acid treatment shows type II nitrogen adsorption isotherm at relative pressures ( $P/P_0$ ) from 0.4 to 1.0. A similar type of nitrogen adsorption isotherm was observed for CMK–PANi

Table 1 BET surface area, pore volume and average pore diameter for the synthesized materials

Sample	BET surface area ( $\text{m}^2/\text{g}$ )	Pore volume ( $\text{cm}^3/\text{g}$ )	Average pore diameter ( $\text{Å}$ )
CMK-3	908	0.62	41.66
CMK–PANi	395	0.44	38.82

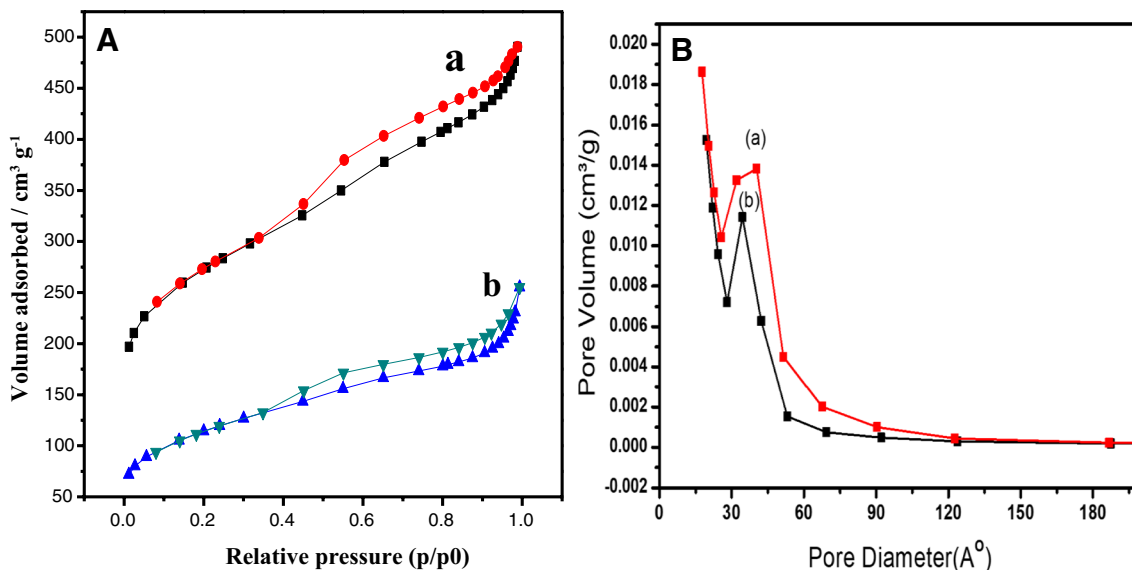


Fig. 4 **A**  $N_2$  adsorption–desorption isotherms of (a) CMK-3 and (b) CMK–PANi composite. **B** Pore size distribution curve of (a) CMK-3 and (b) CMK–PANi composite

composite at relative pressures from 0.4 to 1.0 with a decrease in BET surface area due to the confinement of polyaniline inside the CMK-3 and agreed with XRD results of CMK-3 and CMK-PANi composite.

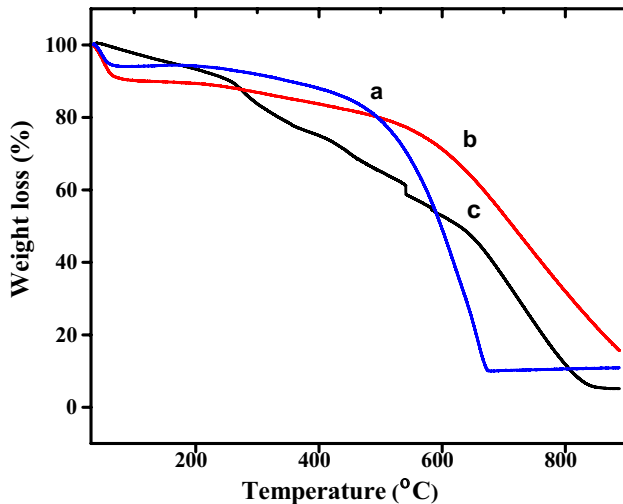


Fig. 5 TGA of (a) PANi, (b) CMK-3 and (c) CMK-PANi composite

Figure 5 shows the TG analysis of PANi, CMK-3 and CMK-PANi composite. TG curve of pure PANi Shows three weight loss at 200 °C, 450 °C and 600 °C which is attributed to the loss of water, degradation of PANi and destruction of PANi respectively. In case of CMK-3 (Fig. 5c) weight loss was observed above 600 °C which is due to the destruction of Carbon in CMK-3 [33]. However, it is worth noting that the CMK-PANi nanocomposite does not have a distinct decomposition temperature and shows a gradual weight loss with increasing temperature. The results depict good thermal stability of CMK-PANi composite because of diffusion constraints in the channel system [36].

Figure 6a, b show SEM images of CMK-3 and CMK-PANi composite. CMK-3 exhibited rod-like particle images which remained unchanged after the in situ polymerization of aniline on CMK-3. Also, the images show the confinement of PANi inside the pores of CMK-3. The TEM images of CMK-3 and CMK-PANi composites shown in Fig. 6c, d, in which CMK-3 shows well-ordered rod-like structures. As in the case of SEM images, TEM images of CMK-PANi composites also show the homogeneous incorporation of PANi over CMK-3. Thus, the results of XRD and BET confirmed the confinement of PANi inside CMK-3.

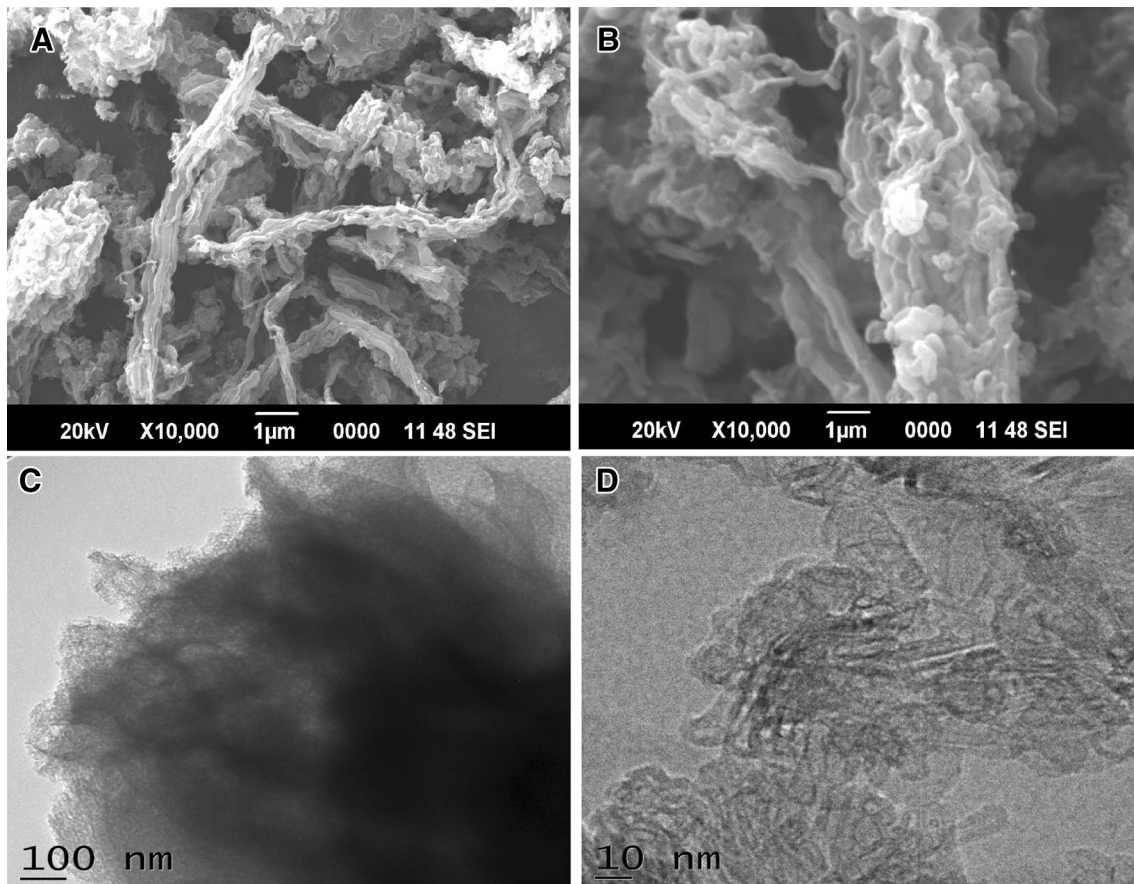


Fig. 6 a SEM image of CMK-3, b SEM image of CMK-PANi composite, c TEM image of CMK-3 and d TEM image of CMK-PANi composite

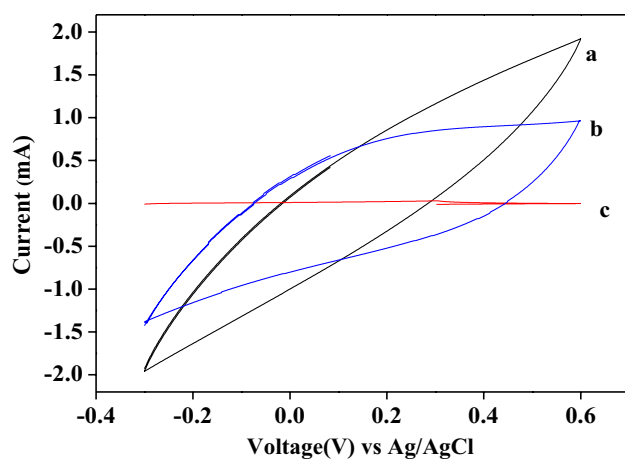


Fig. 7 Cyclic voltammogram of (a) CMK-PANi, (b) CMK-3 and (c) PANi in 1 M  $\text{KHCO}_3$  at 100 mV/s

### 3.2 Electrochemical properties

The synthesized CMK-PANi composite used as electrode material for construction of hybrid capacitors and the electrochemical behaviors were tested in the potential range of  $-0.3$  to  $0.6$  V. The cyclic voltammogram (CV) and impedance studies reveal that the electrochemical capacitance of CMK-PANi composite is due to the formation of an electrical double layer. Figure 7 shows the cyclic voltammogram of CMK-3, PANi, and CMK-PANi in 1 M  $\text{KHCO}_3$  at 100 mV/s scan rate. The CV shapes of the CMK-3 are almost rectangular without redox peaks, which indicate the electric double-layer property of CMK-3. Whereas the CMK-PANi composite shows leaf-like CV graph, which reflects different charge storage capacity. Furthermore, the current response of the CMK-PANi composite was more significant than the CMK-3 and PANi, implying that it has the highest specific capacitance value due to pseudo capacitance and the electric double layer capacitor. Further, redox peaks in the CV curves for the CMK-PANi composite was attributed to the redox transition of PANi between a semiconducting state (leucoemeraldine form) and a conducting state (polaronic emeraldine) [37], that results in the redox capacitance.

Figure 8 shows cyclic voltammogram of CMK-PANi modified electrodes in 1 M  $\text{KHCO}_3$  at different scan rates 1 to 100 mV/s in the potential range of  $-0.3$  to  $0.6$  V. The CMK-PANi material reveals the leaf-like CV curves at different scan rates, and increasing potential with scan rates from 1 to 100 mV/s the current also increases from 0.2 to 2 mA indicates a good rate ability for CMK-PANi [38]. A maximum current of 2 mA was obtained with CMK-PANi electrode, whereas pristine CMK-3 gave about 1 mA, the increase in current indicates the high capacitance of CMK-PANi due to the presence of conducting PANi.

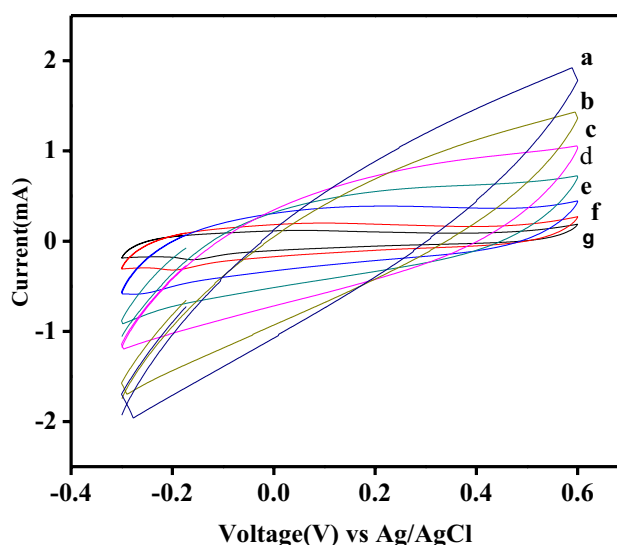


Fig. 8 Cyclic voltammogram of CMK-PANi modified electrodes in 1 M  $\text{KHCO}_3$  at different scan rates (a) 100 mV/s, (b) 50 mV/s, (c) 20 mV/s, (d) 10 mV/s, (e) 5 mV/s, (f) 2 mV/s and (g) 1 mV/s

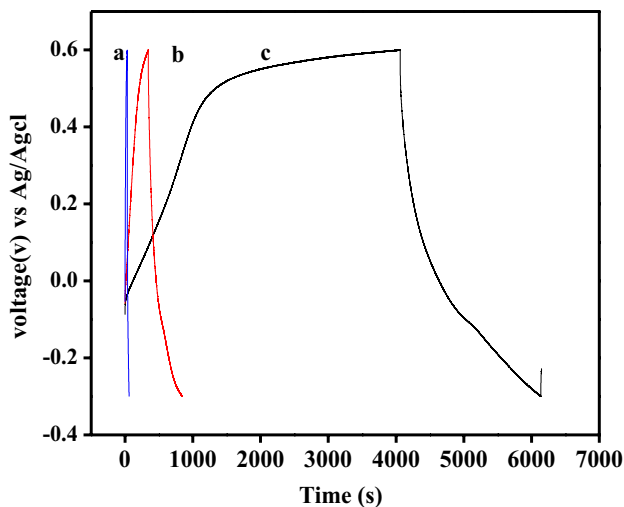
Hence, the PANi facilitates fast ions transport to the surface of electrode materials which enhanced the charge storage capacity. Thus, the uniform confined of PANi on CMK allows high current density with increased storage efficiency.

Figure 9 shows the GCD curve of (a) PANi, (b) CMK-3, (c) CMK-PANi composite at current density 0.2 A/g. The CMK-3 possess an ideal electric double-layer (EDL) capacitor, hence the shape of GCD curve is almost symmetric and small ohmic IR potential drop was observed which indicates that the potential of Helmholtz layer was smaller than the diffuse layer with diluted electrolyte solutions. Also, CMK-PANi composites display no sharp IR drops in  $\text{KHCO}_3$  that indicates the ideal electrochemical reversibility and low equivalent series resistance [39]. The capacitance was calculated from GCD measurements using the following equation.

$$C = \frac{I\Delta t}{m\Delta V}$$

where C is specific capacitance (F/g), I is the charge-discharge current (A), m is the mass of active material (g), t is the discharge time (s), and V is the working voltage (V). From the GCD measurements, CMK-PANi exhibits a higher specific capacitance of 487 F/g at 0.2 A/g, than other reports of PANi/CMK-3 at various current densities [38], this might be due to the influence of bicarbonate ions in the electrolyte.

Figure 10 shows the GCD curve of CMK-PANi composite at different current densities 0.2, 0.4, 0.8, 1.0, and 2 A/g and correspond specific capacitance was 487, 376, 280,



**Fig. 9** GCD curve of (a) PANi, (b) CMK-3 and (c) CMK-PANi composite at current density 0.2 A/g

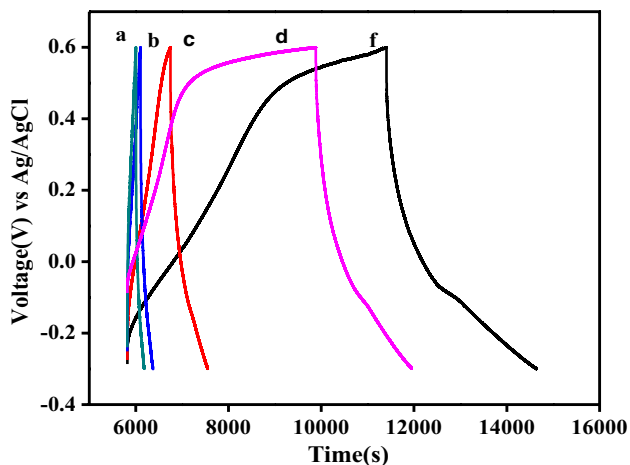


**Fig. 10** GCD curve of CMK-PANi Nano composite at different current densities (a) 0.2 A/g, (b) 0.4 A/g, (c) 0.8 A/g, (d) 1 A/g and (e) 2 A/g

238, and 158 F/g, respectively. The long-term stability of CMK-PANi composites shows better charge-discharge behavior at 0.2 A/g and indicates that CMK-PANi composites are best electrode materials which are in agreement with the CV data. The presence of conducting PANi on high surface mesoporous CMK-3 and the role of  $\text{HCO}_3^-$  have resulted in the high charge-discharge capacity of the CMK-PANi composites.

Figure 11a shows the cyclic performance of CMK-PANi composite, the stability of CMK-3 and CMK-PANi electrodes was measured by repeated charge-discharge at 0.8 A/g. The specific capacitance of pure CMK-3 retains almost 81% after 5000 charge-discharge cycles due to its electrical double layer capacitance. However, the

CMK-PANi electrode shows a slight decrease during first 150 cycles and subsequently keeps stable; this might be attributed due to the structural changes that occur in PANi at a constant current which causes change in the conducting properties of PANi. Figure 11b showed the effect of current density on the specific capacitance of CMK-PANi composite and observed that specific capacitance decreased from 487 to 158 F/g when current density increased from 0.2 to 2 A/g. The decrease in specific capacitance on increasing current densities is due to the higher electrolyte diffuse hindrance that reduces the active site utilization ratio at high current density [40]. However, the CMK-PANi composite shows somewhat appreciable specific capacitance in  $\text{KHCO}_3$  system, when compared to reported composites (Table 2) [38, 42–51].

Figure 11c shows Nyquist plots of CMK-PANi composite from electrochemical impedance spectroscopy (EIS) employed at DC bias of monitor. Nyquist plot, a plot of a frequency response for CMK-PANi composite was obtained with a frequency loop from 1 MHz to 10 kHz. Each impedance curve shows a part of single semicircle in the high-frequency region and a straight line in the low-frequency region. The diameter of semicircle presents the charge-transfer resistance in the electrochemical system. The semicircle diameter of CMK-PANi composite is smaller than that of pure PANi, which indicates that the composite has the lowest electrochemical charge-transfer resistance [41].  $R_s$  is the estimated for CMK-PANi is to be about  $0.25 \Omega$ . The lowest electrochemical charge-transfer resistance in CMK-PANi is due to the resistance of electrolyte solution and also the due to the intrinsic resistance of the active material. Further, CMK-PANi composite displays the internal resistance, which was slightly higher in  $\text{KHCO}_3$  electrolyte, this might be due to the larger diameter of  $\text{HCO}_3^-$  ions compared to  $\text{OH}^-$  or  $\text{SO}_4^{2-}$  ions. Table 2 shows few reports on the combination of the porous carbon and polyaniline, still, no report on the effect of bicarbonate electrolyte with CMK-PANi composite electrode. Thus,  $\text{KHCO}_3$  can be demonstrated as a suitable electrolyte for CMK-PANi composite for this supercapacitor behavior.

## 4 Conclusions

CMK-PANi composite was successfully synthesized using SBA-15 as template and aniline by in situ polymerization technique. XRD and BET analysis revealed the formation of mesoporous materials with the high surface area. The BET data supported porous nature of CMK-PANi after PANi incorporation. IR and Raman spectroscopy revealed confinement of PANi inside the CMK matrix and the formation of disordered graphite carbon. The synthesized CMK-PANi composite was used as an electrode material

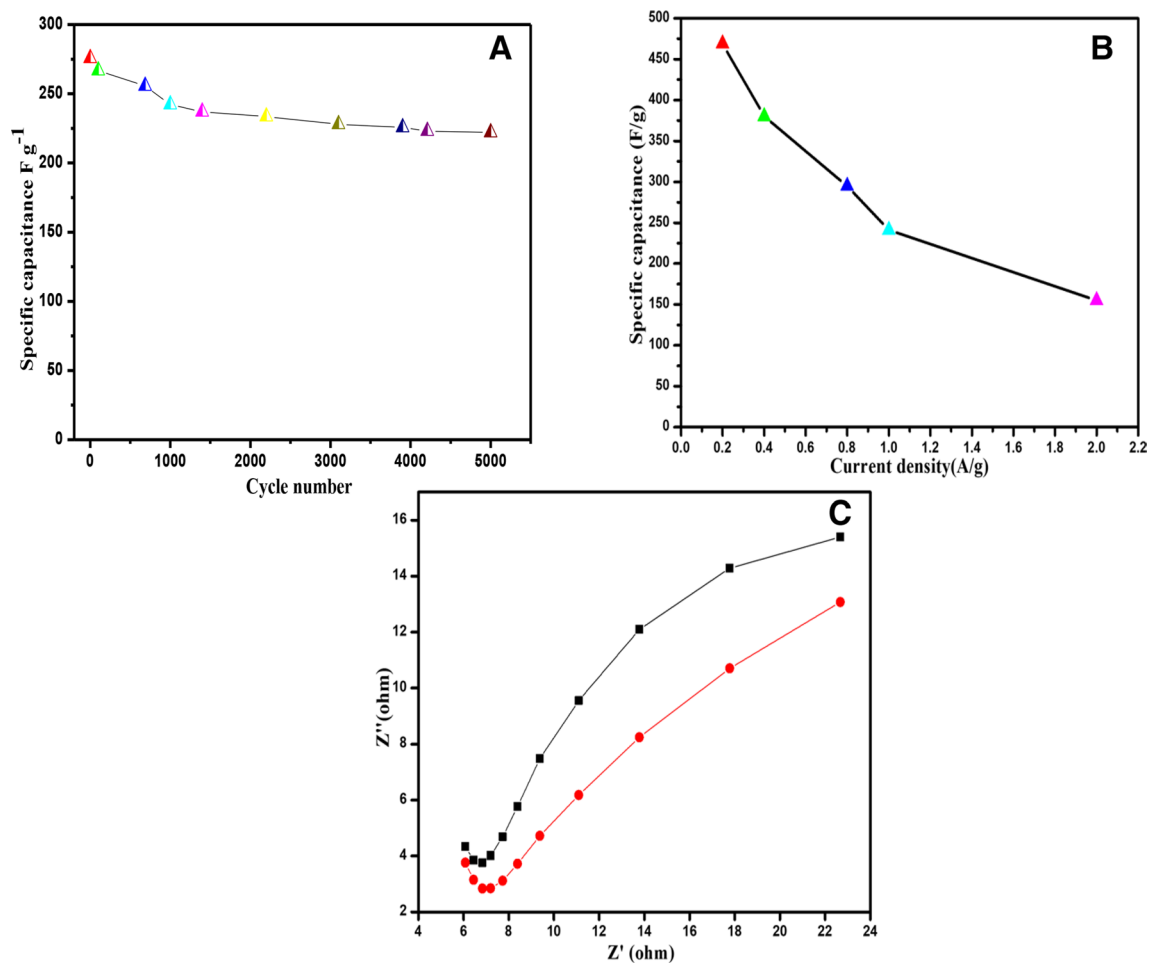


Fig. 11 (a) Cyclic performance at 0.8 A/g, (b) Effect of current density on specific capacitance and (c) Nyquist plots of CMK-PANi composite

**Table 2** Comparisons of the specific capacitance with the various mesoporous carbon-PANi composite

Materials	Specific capacitance (F/g)	Scan rate or current density (A/g)	Electrolyte	References
PANI-NWs/CMK-3	470	1	1 M H <sub>2</sub> SO <sub>4</sub>	[38]
PANI/NOMC	276.1	0.2	2 M KOH	[42]
PANI/CMK-3	87.4	5 mA/cm <sup>2</sup>	1 M H <sub>2</sub> SO <sub>4</sub>	[43]
CMK-5-PANi	803	0.25	2 M H <sub>2</sub> SO <sub>4</sub>	[44]
PANI-F/LMC	473	0.1	6 M KOH	[45]
OMC/PANI	747	0.1	30 wt% KOH	[46]
PANI/MPC	400	1	1 M H <sub>2</sub> SO <sub>4</sub>	[47]
PANI/MC	470	2 mV s <sup>-1</sup>	1 M H <sub>2</sub> SO <sub>4</sub>	[48]
HPC/PANI	1080	1	1 M H <sub>2</sub> SO <sub>4</sub>	[49]
MC/PANI	1500	1	1 M H <sub>2</sub> SO <sub>4</sub>	[50]
PANI/OBMC	517	0.1	1 M H <sub>2</sub> SO <sub>4</sub>	[51]
CMK-PANi	487	0.2	1 M KHCO <sub>3</sub>	This work

to study the supercapacitor behavior in KHCO<sub>3</sub> as electrolyte. CMK-PANi composite exhibited a leaf-like CV graph with large current response that corresponds to

the double layer capacitance, which is also supported by impedance studies. The specific capacitance for CMK-PANi composite at 0.2 A/g in KHCO<sub>3</sub> was 487 F/g. It also retains



90% of capacitance after 1000 charge–discharge cycles. EIS data revealed that CMK–PANi composite also exhibits lowest electrochemical charge-transfer resistance  $\text{KHCO}_3$  electrolyte.

**Acknowledgements** This research was supported by a Grant (SB/FT/CS-119/2013 dated 30.06.2014) from the Science and Engineering Research Board, funded by the Department of Science and Technology of Government of India.

## Compliance with ethical standards

**Conflict of interest** The authors declare that they have no conflict of interest.

## References

1. Conway BE (2013) Electrochemical supercapacitors: scientific fundamentals and technological applications. Springer, Berlin
2. Miller JR, Simon P (2008) Electrochemical capacitors for energy management. *Sci Mag* 321(5889):651–652
3. Reddy T (2010) Linden's handbook of batteries, 4th edn. McGraw-Hill Education, New York
4. Zhai Y, Dou Y, Zhao D, Fulvio PF, Mayes RT, Dai S (2011) Carbon materials for chemical capacitive energy storage. *Adv Mater* 23(42):4828–4850
5. Niu Z, Liu L, Zhang L, Shao Q, Zhou W, Chen X, Xie S (2014) A universal strategy to prepare functional porous graphene hybrid architectures. *Adv Mater* 26(22):3681–3687
6. Ji C-C, Xu M-W, Bao S-J, Cai C-J, Lu Z-J, Chai H, Yang F, Wei H (2013) Self-assembly of three-dimensional interconnected graphene-based aerogels and its application in supercapacitors. *J Colloid Interface Sci* 407:416–424
7. Peng X, Peng L, Wu C, Xie Y (2014) Two dimensional nanomaterials for flexible supercapacitors. *Chem Soc Rev* 43(10):3303–3323
8. Qu Q, Yang S, Feng X (2011) 2D Sandwich-like sheets of iron oxide grown on graphene as high energy anode material for supercapacitors. *Adv Mater* 23(46):5574–5580
9. Tran VC, Kharismadewi D, Shim J-J (2015) Ultralong  $\text{MnO}_2$  nanowires intercalated graphene/ $\text{Co}_3\text{O}_4$  composites for asymmetric supercapacitors. *Mater Lett* 147:123–127
10. Huang H, Gan M, Ma L, Yu L, Hu H, Yang F, Li Y, Ge C (2015) Fabrication of polyaniline/graphene/titania nanotube arrays nanocomposite and their application in supercapacitors. *J Alloys Compd* 630:214–221
11. Xie A, Wu F, Sun M, Dai X, Xu Z, Qiu Y, Wang Y, Wang M (2015) Self-assembled ultralight three-dimensional polypyrrole aerogel for effective electromagnetic absorption. *Appl Phys Lett* 106(22):222902
12. Ye S, Feng J (2014) Self-assembled three-dimensional hierarchical graphene/polypyrrole nanotube hybrid aerogel and its application for supercapacitors. *ACS Appl Mater* 6(12):9671–9679
13. Lamiel C, Kharismadewi D, Tran VC, Shim J-J (2015) Covalently bonded reduced graphene oxide/polyaniline composite for electrochemical sensors and capacitors. *J Electroanal Chem* 758:148–155
14. Stejskal J, Gilbert R (2002) Polyaniline. Preparation of a conducting polymer (IUPAC technical report). *Pure Appl Chem* 74(5):857–867
15. Chiang J-C, MacDiarmid AG (1986) 'Polyaniline': protonic acid doping of the emeraldine form to the metallic regime. *Synth Met* 13(1–3):193–205
16. Qu Y, Lu C, Su Y, Cui D, He Y, Zhang C, Cai M, Zhang F, Feng X, Zhuang X (2018) Hierarchical-graphene-coupled polyaniline aerogels for electrochemical energy storage. *Carbon* 127:77–84
17. Lu X, Dou H, Yang S, Hao L, Zhang L, Shen L, Zhang F, Zhang X (2011) Fabrication and electrochemical capacitance of hierarchical graphene/polyaniline/carbon nanotube ternary composite film. *Electrochim Acta* 56(25):9224–9232
18. Bavio MA, Acosta GG, Kessler T (2014) Synthesis and characterization of polyaniline and polyaniline–carbon nanotubes nanostructures for electrochemical supercapacitors. *J Power Sources* 245:475–481
19. Cheng Q, Tang J, Shinya N, Qin L-C (2013) Polyaniline modified graphene and carbon nanotube composite electrode for asymmetric supercapacitors of high energy density. *J Power Sources* 241:423–428
20. Pieta P, Obratsov I, D'Souza F, Kutner W (2013) Composites of conducting polymers and various carbon nanostructures for electrochemical supercapacitors. *ECS J Solid State Sci Technol* 2(10):M3120–M3134
21. Inagaki S, Yokoo Y, Miki T, Kubota Y (2013) Improvement of electric double-layer capacitance of ordered mesoporous carbon CMK-3 by partial graphitization using metal oxide catalysts. *Microporous Mesoporous Mater* 179:136–143
22. Almeida VC, Silva R, Acerce M, Junior OP, Cazetta AL, Martins AC, Huang X, Chhowalla M, Asefa T (2014) N-doped ordered mesoporous carbons with improved charge storage capacity by tailoring N-dopant density with solvent-assisted synthesis. *J Mater Chem A* 2(36):15181–15190
23. Joo SH, Choi SJ, Oh I, Kwak J, Liu Z, Terasaki O, Ryoo R (2001) Ordered nanoporous arrays of carbon supporting high dispersions of platinum nanoparticles. *Nature* 412(6843):169
24. Liu G, Zheng S, Yin D, Xu Z, Fan J, Jiang F (2006) Adsorption of aqueous alkylphenol ethoxylate surfactants by mesoporous carbon CMK-3. *J Colloid Interface Sci* 302(1):47–53
25. Liu X, Zhou L, Li J, Sun Y, Su W, Zhou Y (2006) Methane sorption on ordered mesoporous carbon in the presence of water. *Carbon* 44(8):1386–1392
26. Ding J, Chan K-Y, Ren J, Xiao F (2005) Platinum and platinum–ruthenium nanoparticles supported on ordered mesoporous carbon and their electrocatalytic performance for fuel cell reactions. *Electrochim Acta* 50(15):3131–3141
27. Nam J-H, Jang Y-Y, Kwon Y-U, Nam J-D (2004) Direct methanol fuel cell Pt–carbon catalysts by using SBA-15 nanoporous templates. *Electrochim Commun* 6(7):737–741
28. Vinoba M, Bhagiyalakshmi M, Jeong SK, Yoon YI, Nam SC (2012) Carbonic anhydrase conjugated to nanosilver immobilized onto mesoporous SBA-15 for sequestration of  $\text{CO}_2$ . *J Mol Catal B Enzym* 75:60–67
29. Zhao D, Feng J, Huo Q, Melosh N, Fredrickson GH, Chmelka BF, Stucky GD (1998) Triblock copolymer syntheses of mesoporous silica with periodic 50 to 300 angstrom pores. *Science* 279(5350):548–552
30. Ryoo R, Joo SH, Kruk M, Jaroniec M (2001) Ordered mesoporous carbons. *Adv Mater* 13(9):677–681
31. Jun S, Joo SH, Ryoo R, Kruk M, Jaroniec M, Liu Z, Ohsuna T, Terasaki O (2000) Synthesis of new, nanoporous carbon with hexagonally ordered mesostructure. *J Am Chem Soc* 122(43):10712–10713
32. Zhu S, Gu J, Chen Z, Dong J, Liu X, Chen C, Zhang D (2010) Controlled synthesis of polyaniline inside mesoporous carbon for electroanalytical sensors. *J Mater Chem* 20(24):5123–5128
33. Anbia M, Salehi S (2016) Synthesis of polyaniline/mesoporous carbon nanocomposites and their application for  $\text{CO}_2$  sorption. *J Polym Res* 23(7):124

34. Shim J-W, Park S-J, Ryu S-K (2001) Effect of modification with  $\text{HNO}_3$  and  $\text{NaOH}$  on metal adsorption by pitch-based activated carbon fibers. *Carbon* 39(11):1635–1642
35. Ahmed A, Siddique MN, Ali T, Tripathi P (2018) Influence of reduced graphene oxide on structural, optical, thermal and dielectric properties of  $\text{SnO}_2$  nanoparticles. *Adv Powder Technol* 29:3415–3526
36. He Y, Cheng Q, Pavlinek V, Li C, Saha P (2008) Synthesis and structural characterization of polyaniline/mesoporous carbon nanocomposite. *Int J Polym Anal Charact* 13(1):25–36
37. Du W, Wang X, Sun X, Zhan J, Zhang H, Zhao X (2018) Nitrogen-doped hierarchical porous carbon using biomass-derived activated carbon/carbonized polyaniline composites for supercapacitor electrodes. *J Electroanal, Chem*
38. Yan Y, Cheng Q, Wang G, Li C (2011) Growth of polyaniline nanowhiskers on mesoporous carbon for supercapacitor application. *J Power Sources* 196(18):7835–7840
39. Wang D, Fang G, Xue T, Ma J, Geng G (2016) A melt route for the synthesis of activated carbon derived from carton box for high performance symmetric supercapacitor applications. *J Power Sources* 307:401–409
40. Chang J, Gao Z, Zhao W, Guo L, Tang Y, Wu D, Xu F, Jiang K (2016) Nitrogen doped microporous carbons with tunable and selective performances in supercapacitor and heterogeneous catalysis. *Electrochim Acta* 190:912–922
41. Yan Y, Cheng Q, Pavlinek V, Saha P, Li C (2012) Fabrication of polyaniline/mesoporous carbon/ $\text{MnO}_2$  ternary nanocomposites and their enhanced electrochemical performance for supercapacitors. *Electrochim Acta* 71:27–32
42. Xie K, Zhang M, Yang Y, Zhao L, Qi W (2018) Synthesis and supercapacitor performance of polyaniline/nitrogen-doped ordered mesoporous carbon composites. *Nanoscale Res Lett* 13(1):163
43. Cai JJ, Kong LB, Zhang J, Luo YC, Kang L (2010) A novel polyaniline/mesoporous carbon nano-composite electrode for asymmetric supercapacitor. *Chin Chem Lett* 21(12):1509–1512
44. Lei Z, Sun X, Wang H, Liu Z, Zhao X (2013) Platelet CMK-5 as an excellent mesoporous carbon to enhance the pseudocapacitance of polyaniline. *ACS Appl Mater Interfaces* 5(15):7501–7508
45. Liu H, Xu B, Jia M, Zhang M, Cao B, Zhao X, Wang Y (2015) Polyaniline nanofiber/large mesoporous carbon composites as electrode materials for supercapacitors. *Appl Surf Sci* 332:40–46
46. Li L, Song H, Zhang Q, Yao J, Chen X (2009) Effect of compounding process on the structure and electrochemical properties of ordered mesoporous carbon/polyaniline composites as electrodes for supercapacitors. *J Power Sources* 187(1):268–274
47. Dou Y-Q, Zhai Y, Liu H, Xia Y, Tu B, Zhao D, Liu X-X (2011) Syntheses of polyaniline/ordered mesoporous carbon composites with interpenetrating framework and their electrochemical capacitive performance in alkaline solution. *J Power Sources* 196(3):1608–1614
48. Zhou S, Mo S, Zou W, Jiang F, Zhou T, Yuan D (2011) Preparation of polyaniline/2-dimensional hexagonal mesoporous carbon composite for supercapacitor. *Synth Met* 161(15–16):1623–1628
49. Yu P, Zhang Z, Zheng L, Teng F, Hu L, Fang X (2016) A novel sustainable flour derived hierarchical nitrogen-doped porous carbon/polyaniline electrode for advanced asymmetric supercapacitors. *Adv Eng Mater* 6(20):1601111
50. Li J, Ren Y, Ren Z, Wang S, Qiu Y, Yu J (2015) Aligned polyaniline nanowires grown on the internal surface of macroporous carbon for supercapacitors. *J Mater Chem A* 3(46):23307–23315
51. Yan Y, Cheng Q, Zhu Z, Pavlínek V, Saha P, Li C (2013) Controlled synthesis of hierarchical polyaniline nanowires/ordered bimodal mesoporous carbon nanocomposites with high surface area for supercapacitor electrodes. *J Power Sources* 240:544–550

**Publisher's Note** Springer Nature remains neutral with regard to jurisdictional claims in published maps and institutional affiliations.